Thermal Impedance in Pulsed Energy Storage Systems with Phase Change Materials

Juan C. Lago
Veronica Gonzalez
Alison Hoe
Michael Barako
Patrick J. Shamberger

[1] Department of Materials Science and Engineering
Texas A&M University
College Station, TX, 77843, USA

[2] NG Next Basic Research Laboratory
Northrop Grumman Corporation
Redondo Beach, CA, 90278, USA

Phone: 979-458-1086
Fax: 979-862-6835
E-mail: patrick.shamberger@tamu.edu

Highlights

- The concept of thermal impedance offers insights into the time scale at which heat can be injected into extracted from a thermal storage reservoir.
- Thermal impedance is strongly non-linear in a relatively narrow range of duty factor/pulse on time/power conditions.
- Experimentally measured thermal impedance of paraffin-infiltrated copper foams show general agreement with ideal composite behavior.

Abstract

Phase change materials (PCMs) have tremendous capacity as passive components to recover and repurpose thermal energy from transient power systems. However, PCMs are only effective if the time scale of the thermal energy storage and retrieval rates match those required for a particular system. We develop a framework to assess the efficiency of pulsed thermal energy storage based on the concept of "thermal impedance", drawing upon an analogous approach from electrical energy storage. We experimentally characterize a paraffin-infiltrated copper foam composite PCM, and demonstrate a decrease in thermal impedance over a narrow range of operating conditions which represents both a signature of the ability to extract or retrieve thermal energy via latent heat, as well as an experimentally accessible measure that provides insight into the internal dynamics of a composite PCM volume. These principles can serve to design the internal structure of composite PCM elements for pulsed thermal systems.

Main

Energy storage devices function as temporary reservoirs that bridge time gaps between energy generation and use. These devices use materials and architectures engineered to facilitate rapid and recoverable energy exchange. Examples include devices designed to store energy in the form of electrical fields (dielectrics for capacitors),[1] electrochemical potential (battery electrodes),[2] kinetic energy (flywheel mass),[3] thermophysical energy (high heat capacity materials), or thermochemical energy (reversible hydration-dehydration media).[4] To effectively store a transient pulse of energy, the time scale of the storage device must have sufficient bandwidth to absorb the pulse, rather than rejecting it through dissipative pathways or raising the temperature of the source. This energy storage bandwidth may be limited by rates of charge transport and energy conversion, as exemplified by the charge/discharge rates of electrochemical batteries,[2] or by the rates of heat and mass transfer within the device, as exemplified by thermochemical energy storage systems.[5,6] While energy storage rate bottlenecks have received much attention for electrochemical systems,[2,7-9] they remain a critical bottleneck in advancing thermal energy storage materials and components.

It remains challenging to characterize the energy storage bandwidth across time scales and driving potentials, which is necessary to develop effective components tailored for a particular system. While the use of Ragone plots based on intrinsic materials properties and figures of merit[10,11] and the thermal rate capability framework[12] introduce a framework to evaluate thermal energy storage materials and components under quasi-steady loads, there remains no systematic framework to evaluate the thermal response of a phase change material (PCM) nonlinear storage element to periodic unsteady loading and unloading cycles. In contrast, the equivalent response to a nonlinear electrical energy storage device (its electrical impedance) has been broadly adopted as a strategy to characterize energy storage kinetics and to effectively incorporate these elements into both design strategies and the analysis of complex circuits. By analogy, we extrapolate from this approach to define a thermal impedance as a system characteristic that comprehensively captures material, geometric, and temporal effects on the time-varying thermal response of nonlinear PCMs. This strategy enables the design, optimization, and

operation of PCMs at the minimum impedance, which maximizes the capacity for energy exchange between the storage medium and the adjacent sources and sinks.

In purely electrical systems, energy is stored either through the accumulation of charge (capacitance) or in the form of electromagnetic fields that oppose changes in current (inductance). Electrical impedance is defined as the ratio of the complex bias to the complex current,

$$Z_{\mathrm{el}} = V/I, \qquad \text{Eq. 1}$$

This quantity describes the opposition of an electronic circuit to current by the combined resistance and reactance of the circuit. Critically, electrical impedance offers a rigorous framework to evaluate the ability of an individual component or a collection of components to transmit and accumulate electrical energy at different time scales. In more complicated electrochemical systems, electrical impedance measurements offer a means of quantifying the rates associated with fundamental processes that represent bottlenecks to storage of electrochemical energy (e.g., double-layer and space charge capacitance,[13] charge transfer and chemical diffusion[14,15]). As such, electrochemical impedance spectroscopy offers an invaluable technique to measure kinetics of both transient and steady state processes in batteries and related electrochemical systems.[16]

By analogy, thermal circuits and purely thermal energy storage systems are subject to equivalent rate limitations. A thermal storage device exhibits a resistance to heat flow across its boundaries due to a combination of internal resistance, and thermal capacitance or accumulation of thermal energy in sensible and latent forms. Thus, a thermal impedance, Z_{th}, may also be defined as the ratio of the thermal bias to the thermal current (heat transfer rate):

$$Z_{\mathrm{th}} = \Delta T/\dot{Q}_0, \qquad \text{Eq. 2}$$

Despite these similarities, the framework of thermal impedance has primarily been applied to describe the ability of components to transmit heat (Fig. 1c, ‘transmitted’) rather than their capacity to accumulate thermal energy (Fig. 1c, ‘stored/latent heat’). As examples, thermal impedance has been introduced as a technique to characterize the thermal transfer functions and characteristic heat transfer behavior within electronics packages,[17-19] and in different electrochemical systems (including batteries,[20,21] capacitors,[22] and even buried power cables[23]). In these examples, the concept of thermal impedance is primarily used to convey a resistance to removing heat generated within a system, resulting in transient temperature spikes. However, in either a thermally grounded or an adiabatic configuration, low thermal impedance can also result from accumulation of thermal energy within a thermal energy storage material.

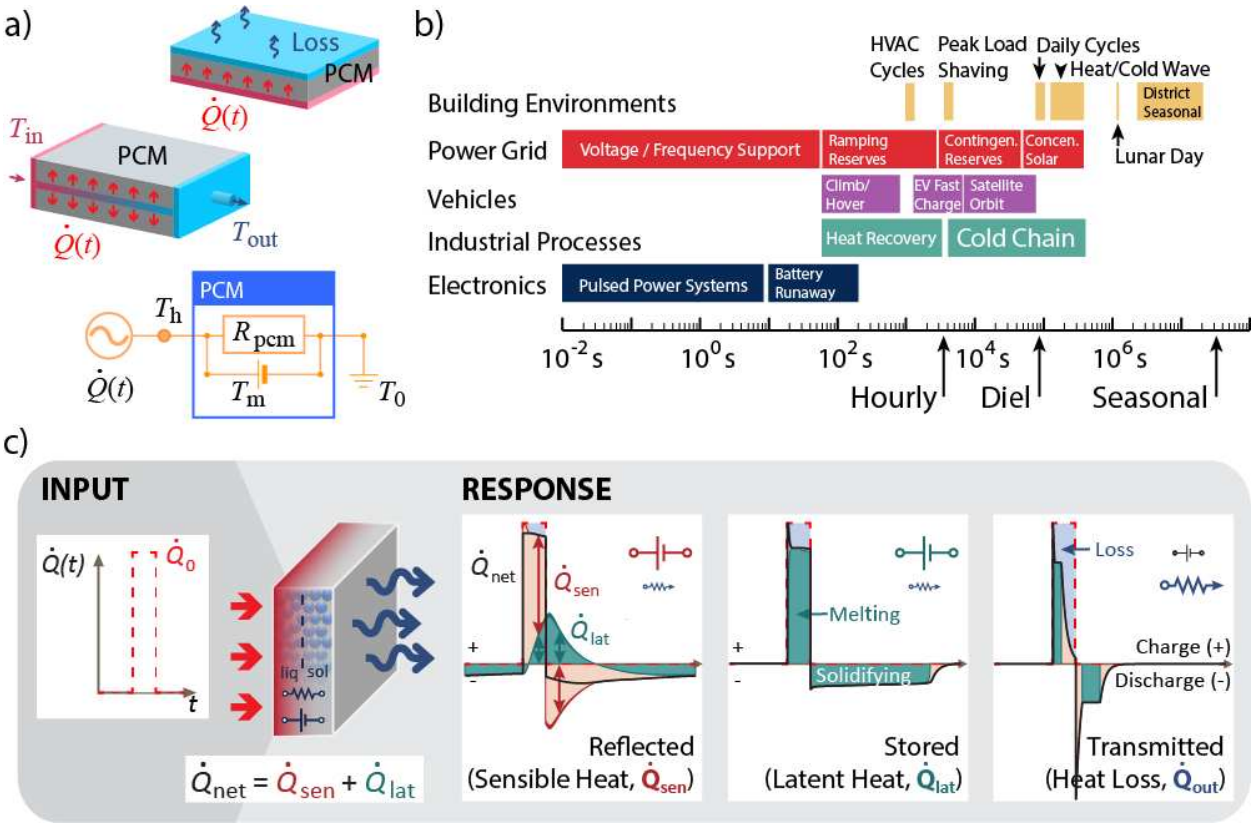

Fig. 1. a) Generic thermal energy storage volumes and thermal circuit representing a PCM thermal energy storage element in series between a heat source and heat sink. b) Thermal energy storage applications bridge a wide range of time scales from thermal management of short electronic pulses to seasonal energy storage concepts, which dictate the optimal response time of a thermal energy storage component. c) In response to an input pulse of thermal energy, $\dot{Q}_0$, heat can either be dissipated (lost), $\dot{Q}_{out}$, or can be stored within the volume, $\dot{Q}_{net}$, where energy balance dictates $\dot{Q}_{net} = \dot{Q}_0 - \dot{Q}_{out}$. The net heat stored can be partitioned into sensible and latent heat components: $\dot{Q}_{net} = \dot{Q}_{sen} + \dot{Q}_{lat}$. Here we represent three characteristic regimes, where the dominant term is $\dot{Q}_{sen}$, $\dot{Q}_{lat}$, or $\dot{Q}_{out}$; the characteristic response depends on 1) thermal boundary conditions, 2) time scale of the input heat pulse (**Fig. 4**), 3) geometry of the system, and 4) intrinsic material properties of the thermal energy storage media.

Thermal energy storage systems designed for periodic steady or pulsed power loads bridge over ten orders of magnitudes of time scales (Fig. 1a), introducing significant challenges in matching the rate of heat accumulation and rejection at both low and high charge / discharge periods. Long period thermal energy storage systems (hours, days, months) include seasonal energy storage (district thermal storage solutions,[24,25] greenhouse thermal management,[26] and geological thermal reservoirs[27]), and diel cycles (concentrated solar power[28,29], building climate control systems[30,31]), both of which tend to require either well insulated systems or alternatively thermochemical energy storage strategies where reactants can be physically separated to avoid premature release of stored thermal energy, to reduce loss terms, $\dot{Q}_{out}$. Industrial and vehicular applications (industrial waste heat recovery, electric vehicle battery charging and discharging, satellite applications), tend to occupy intermediate periods (minutes, hours), whereas electronic or optoelectronic components (pulsed power electronic devices or electro-optical packages[32,33]) occur with sub-second to sub-millisecond bursts. For short period energy storage,

opportunities to capture and re-utilize thermal energy generally become more challenging due to limitations in accumulating heat quickly enough without requiring significant overheating to drive the thermal storage process. At both extremes, frequency mismatch between the time scale of the thermal process and the natural time scale of the storage system can result in inefficiencies including excessive over-heating or loss of heat to the surrounding environment. However, thermal impedance serves as a governing framework to both understand critical rate-limiting mechanisms and design appropriate components to match the storage time scales, much like design strategies that have been implemented for components subjected to steady state boundary conditions.[34-36]

The concept of thermal impedance associated with heat conduction through single-phase solids with periodic heating boundary conditions has been illustrated previously for semi-infinite media.[18,37] As this analysis is limited to thermal resistances and heat capacity, its relevance is limited primarily to sensible heat storage systems. The inclusion of phase change or other latent heat storage elements is significantly complicated by the nonlinear nature of the phase transition. In these cases, numerical and experimental studies have investigated experimental responses to harmonic boundary conditions and identified anti-resonance features associated with thermal buffering of the heated surface.[38,39] While harmonic boundary conditions have advantages in terms of signal processing, and can be analyzed in terms of signal attenuation and phase delay, they are limited in their ability to describe general pulsed power sources which are characterized by both a characteristic time scale and a characteristic duty factor.

Here, we describe a general strategy to characterize and analyze thermal impedance in both linear thermal elements and nonlinear first-order phase transitions exhibited by common PCMs. We experimentally evaluate the thermal impedance of a composite phase change material slab located between a pulsed periodic heat source and an isothermal cold sink. To interpret this data, we calculate both marginal utilization – the fraction of the slab that is melted during each pulse – and the storage fraction – the ratio of the heat absorbed by latent heat of melting each cycle to the quantity of energy in each pulse. We demonstrate that the storage fraction correlates strongly with the impact of a PCM volume on thermal impedance, whereas marginal utilization indicates the upper bound on the pulse length at which an element is able to absorb thermal energy through latent heat. The results demonstrate the utility of thermal impedance as an indirect measure of the impact of the internal structure of the composite on its transient thermal response, which offers critical insight into the design of responsive composite PCM elements for pulsed power systems. Finally, we demonstrate the utility of this concept by combining the thermal impedance of nonlinear PCM elements with simple linear elements (massless resistors) in thermal circuits, offering a pathway to apply this concept to more complex systems.

Theory

The concept of thermal impedance can be intuited by examining the nature of the time-varying temperature on a heated boundary of a slab of material without a phase transition and one-dimensional heat transfer (Fig. 2.). From the perspective of the boundary, more heat will transfer into a material with lower impedance, whether by conduction through the volume, storage within the volume, or some combination thereof. The surface at $x = 0$ is heated with a pulsed periodic waveform $\dot{Q}''(t)$, where each period of length τ_{period} consists of an 'on' heating pulse of constant heat flux $\dot{Q}_0''$ for time τ_{on} and an 'off'

pulse of zero heat input for time τ_{off}. The duty factor $D = \tau_{on}/\tau_{period}$ is the fractional 'on' time for each period, where the limit $D \to 0$ represents a single-pulse with infinite recovery time to ensure the domain returns to the initial temperature T_0 after each pulse. As D increases toward unity, temperature accumulation from the previous pulses begin to affect the heat transfer rate of the current pulse. The opposite surface is a heat sink held isothermal at $T(x = L) = T_0$. The temperature at the heated surface $T(x = 0, t)$ varies in time and is the response function of interest for much of the subsequent analysis, in part because it represents an experimentally accessible measure of the dynamics of the system. The thermal response for a linear, single-phase material depends only on the thermal conductivity k and volumetric heat capacity of the material C_v. When nonlinearities are introduced, such as those associated with a phase change process, where the position of a melting front is not a prescribed boundary, but rather a free boundary, the thermal response becomes coupled to the specific temperatures, heat loads, and time scales.

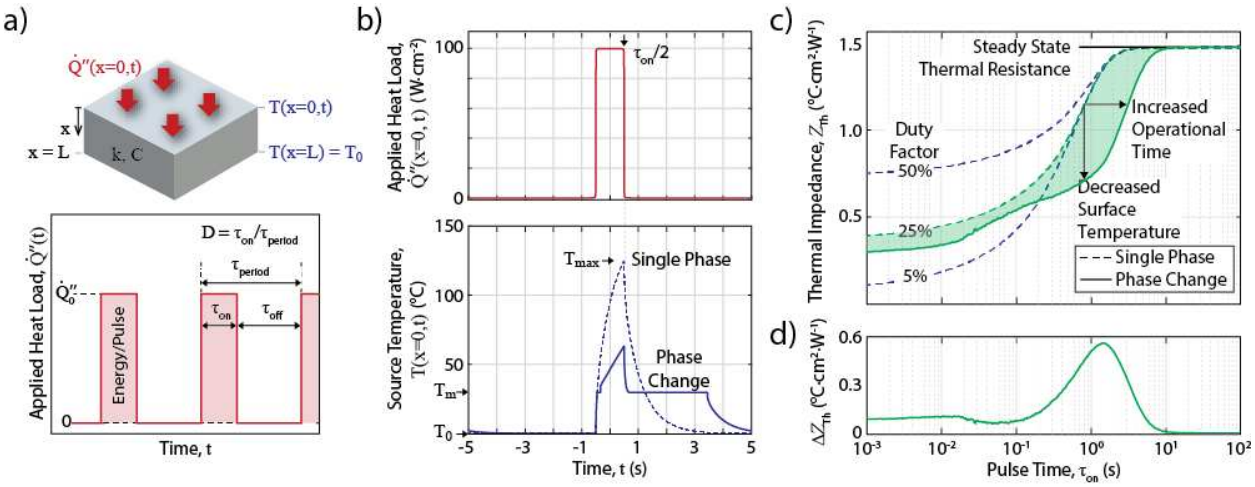

Fig. 2. a) Definition of variables and boundary conditions for model system domain. b) Example heating function and associated temperature response for a 5 mm-thick slab of gallium, where the 'single phase' reference response indicates that the case where melting does not occur (latent heat is set to zero). c) Corresponding thermal impedance for the two cases, where the filled region shows the effect of latent heat energy storage through melting. d) Difference in Z_{th} between a system entirely in the single phase state or that goes through a phase change, which serves as an indicator for the bandwidth of the component.'

Thermal capacitance, Z_{th} (Eq. 2), provides an additional mechanism for heat 'transport' during pulsed power operation by storing energy in concert with transmitting energy. For a system subject to a pulsed heat flux boundary condition, $T_{max} = T(x = 0, t = \tau_{on}/2)$ is the maximum temperature of the heated boundary during steady-periodic operation (i.e., after sufficient periods to eliminate any initial settling transients) and occurs at the end of the heating pulse (Fig. 2b). If the duration of the heating pulse τ_{on} is sufficiently long to reach steady state, or if the duty factor D approaches unity, the capacitive channel can no longer store additional heat and the thermal impedance converges to the steady-state thermal resistance.

In the linear slab described above (the single phase case), the thermal impedance can be defined from the analytical solution to the heat diffusion equation. The governing heat diffusion equation and associated boundary conditions shown in Fig. 2(a) are given by:

$$\frac{\partial T}{\partial t} = \alpha \frac{\partial^2 T}{\partial x^2}, \quad \text{Eq. 3a}$$

$$T(x = L, t) = T_0, \quad \text{Eq. 3b}$$

$$-k \frac{\partial T}{\partial x}\Big|_{x=0} = \dot{Q}''(t), \quad \text{Eq. 3c}$$

where $\alpha = k/C_V$ is the thermal diffusivity. The time-varying heat flux on the heated boundary of the slab is a pulsed periodic waveform of magnitude $\dot{Q}_0''$, with the repeating period τ_{period} defined as:

$$\dot{Q}''(t) = \begin{cases} \dot{Q}_0'' & |t| \le \tau_{on}/2 \\ 0 & |t| > \tau_{on}/2 \end{cases}, -\frac{\tau_{period}}{2} < t < \frac{\tau_{period}}{2}, \quad \text{Eq. 4}$$

where τ_{on} is the pulse duration.

The heating boundary condition given by Eq. 4 can be expressed as a Fourier series:

$$\dot{Q}''(t) = \sum_{n=0}^{\infty} a_n \cos(n\omega_0 t), \dot{Q}(t) = \sum_{n=0}^{\infty} a_n \cos(n\omega_0 t), \quad \text{Eq. 5a}$$

$$a_0 = \dot{Q}_0'' D;\ a_n = \frac{2\dot{Q}_0}{n\pi} \sin\left(n\pi \frac{\tau_{on}}{\tau_{period}}\right) for\ n > 1, \quad \text{Eq. 5b}$$

where $D = \tau_{on}/\tau_{period}$ is the duty factor and $\omega_0 = 2\pi/\tau_{period}$ is the characteristic frequency. We solve for the temperature response on the heated boundary by adding together the temperature response from the individual harmonic heating components. For a single heating frequency ω_n at the heated boundary, the time-varying temperature response is given by:

$$T(x = 0, t, \omega_n) = \frac{\dot{Q}_0 L}{k} \mathrm{Re}\left[\frac{1-e^{-2\sigma}}{\sigma(1+e^{-2\sigma})} e^{i\omega_n t}\right], \quad \text{Eq. 6}$$

where the complex parameter is given by $\sigma = (1+i)\sqrt{\omega_n L^2/2\alpha}$. We then solve for the thermal response of the slab under each harmonic term in Eq. 5 using Eq. 6. Since this is a linear system, the total temperature response at the heated boundary is given by the superposition of harmonic solutions, and the thermal impedance Z_{th} is calculated from Eq. 2, where $\Delta T = T_{\max} - T_0$, using the maximum temperature $T_{max} = T(x = 0, t = \tau_{on}/2)$.

The thermal impedance Z_{th} of a material undergoing a phase change requires a numerical forward-solver to compute the peak temperature response T_{max}. We use a numerical routine previously reported to generate the thermal impedance as a function of both the pulse duration τ_{on} and the duty factor D for a given applied heat flux $\dot{Q}_0''$.[34,40,41] This numerical characteristic can be compared to the analytical solution for a single phase material (i.e., the phase change material which remains in the solid state), and the space separating the two characteristics denotes the region where the latent heat is providing

effective capacitive cooling as shown in Fig. 2c. In the example shown in Fig. 2, a 5 mm-thick slab of gallium is heated by steady-periodic pulses of magnitude $\dot{Q}_0''$ = 100 W·cm^{-2}, and the thermal response is shown with the latent heat term included (numerical solution) and without the latent heat term (Eq. 6). For long pulse durations, the system approaches steady state and the thermal impedance converges to the thermal resistance. For short pulse durations, the sensible heat capacity suppresses the temperature rise below the phase transition and melting never initiates. The region between identifies the effective operational window for this specific phase change system, where the heat source can either operate below the same peak temperature T_{max} for a longer pulse duration τ_{on} or with a lower peak temperature for the same pulse duration.

What conditions promote charging and discharging of heat by a PCM?

For a PCM to efficiently charge and discharge heat via latent heat storage (phase change), three criteria must be satisfied: 1) the temperature of the heated surface must exceed the phase transition temperature T_m, i.e., $T(x=0) > T_m$ to utilize its latent heat, while the temperature of the cooled surface is maintained below T_m, allowing the system to recharge, 2) a significant fraction of the PCM must change phase during each pulse of heat, and 3) the energy absorbed/released by the phase change is a significant overall fraction of the energy in the heat pulse (i.e., heat is neither reflected by nor transmitted through the PCM volume). For sensible heat storage (single phase material) the final point is still relevant, but we will focus here on heat stored as latent heat, as it represents the key capability of PCMs. Since the temperature at the boundary is a direct response to the ability to store heat within the PCM, the above criteria generally correspond to a minimization of thermal impedance. Here we consider the example of "charging" a PCM, i.e., storing heat, but a complimentary set of equivalent criteria can be used to describe "discharging" a PCM, i.e., releasing heat.

The first criteria, $T(x=0) > T_m$, constrains the minimum time scale for absorbing heat by melting, which corresponds with an inflection point in the thermal impedance of a PCM, Z_{th}^{pcm}, as the temperature at the heated surface is held near T_m (e.g., Fig. 2c; τ_{on} = 10^{-1} s). If $T_0 \ll T_m$, heat will be stored only through sensible heating until the surface has heated to the melting point, at which point the phase change mechanism will first be accessed. The maximum effectiveness of a PCM occurs when the temperature of the heated surface first exceeds T_m.

The second criteria defines the fraction of total available PCM that melts (or solidifies) during each cycle. We define a 'marginal utilization factor' U as a metric to indicate the extent to which the phase change process is leveraged:

$$U = Q_{lat}/Q_{pcm,tot}, \qquad \text{Eq. 7}$$

where Q_{lat} is the integral heat absorbed by melting of the PCM each pulse, and $Q_{pcm,tot}$ represents the latent heat content of the whole PCM layer. A low marginal utilization factor occurs when either insufficient melting of the PCM leads to unused available capacity in the thermal energy storage medium or incomplete recovery prevents the PCM from sufficiently discharging its stored heat before the next heat pulse. In the limit $U \to 0$, no energy is stored via latent heat and the PCM does not serve

its intended purpose. In the limit $U \to 1$, the PCM is fully melted and any excess energy input must be stored in sensible heating, which creates an additional temperature rise.

The third criteria describes the ratio of heat absorbed during melting to the total heat pulse. We define and calculate a 'storage fraction' to relate the experimentally observable $Z_{\mathrm{th}}^{\mathrm{pcm}}$ to the relative ratio of heat that is stored for a specific heat pulse,

$$S = Q_{\mathrm{lat}}/Q_{\mathrm{pulse}}, \qquad \text{Eq. 8}$$

where $Q_{\mathrm{pulse}} = \dot{Q}_0 \tau_{\mathrm{on}}$ is the total energy in a single heat pulse. Excess energy that is not stored via latent heat is either transmitted or stored via sensible heating resulting in a corresponding temperature rise, which increases Z_{th}.

Experimental system of study

To experimentally validate the concept of nonlinear thermal impedance in a phase change material (PCM) layer, we evaluated a composite PCM consisting of a high porosity (ϕ = 0.967, 31 PPI; Fig. SI-1, SI-2) open cell copper foam infiltrated with hexadecane. This system was selected because of its relatively high effective thermal conductivity (4.8 $W{\cdot}m^{-1}{\cdot}K^{-1}$; Fig. SI-3, SI-4), combined with the reasonably high volumetric enthalpy of fusion of hexadecane (181.5 $J{\cdot}cm^{-3}$)[42] which together indicate the ability to store pulses of heat at relatively fast rates.[10,11] This measurement apparatus is assembled as a 1D measurement, with a periodic heat source (a thin film heater) on the top surface and a nominally-isothermal cold plate on the bottom surface (Fig. 3).

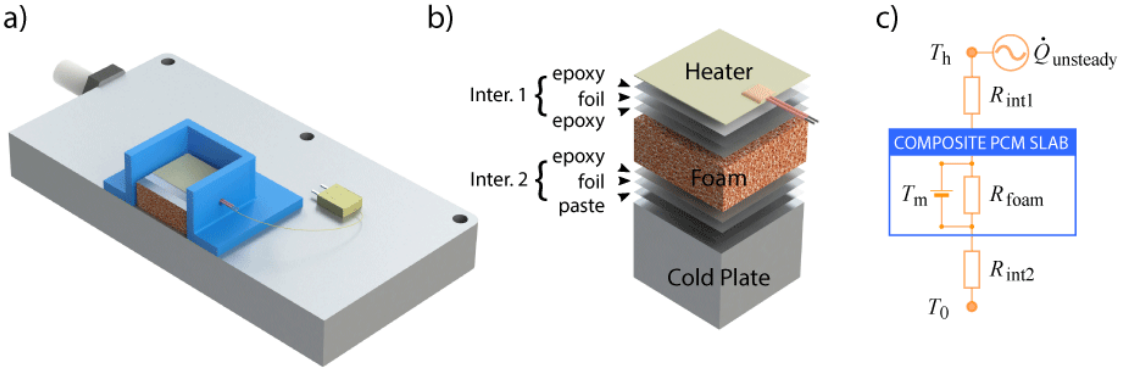

Fig. 3. System of study investigated experimentally. a) Schematic of the test setup constructed directly on a cold plate, including blue housing which contains the liquid PCM. b) Cross-section of the test setup, illustrating the sequence of thermally conductive epoxy/paste and foil as heat spreaders at interface 1 and 2. T_h is measured by a thermocouple bonded to the top surface of the foil in interface 1, T_0 is measured on the top surface of the cold plate. c) Simplified thermal circuit, illustrating interfacial resistances, and the composite PCM slab including a storage component in parallel with a resistive component.

Thermal impedance due to melting of a PCM

Thermal impedance is measured for both an unfilled copper foam, which responds as a linear resistor-capacitor (Fig. SI-5, SI-6), and for a hexadecane/copper foam composite. We perform measurements over a range of duty factors from the single pulse limit (D = 0) with arbitrarily long recovery periods to an even duty cycle (D = 0.5) with incomplete recovery between pulses. We measure pulse times from short bursts that are absorbed into the material as though it were semi-infinite (τ_{on} = 10^{-2}) to long on-time durations that approach steady state and the linear thermal resistance ($\tau_{on} > 10^2$) (Fig. 4). During operation where the PCM undergoes a phase transition, the heating curve is observed to inflect, and the maximum temperature rise is suppressed by endothermic melting (Fig. 4b, 4c). After a sufficient period has passed to establish a regular periodic thermal response, the thermal impedance, Z_{th}, is calculated using Eq. 2. In materials without a phase transition (e.g., unfilled copper foam), the surface temperature rise scales with $\dot{Q}_0''$ resulting in a constant Z_{th} (Fig. SI-6), whereas the introduction of melting introduces nonlinear scaling behavior.

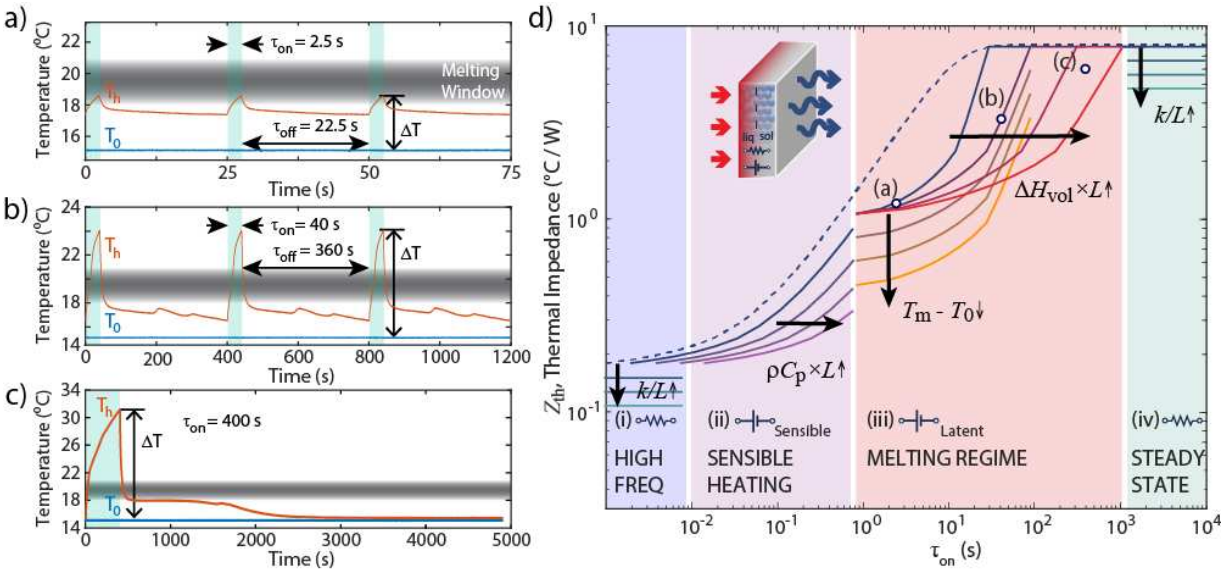

Fig. 4. Periodic response of composite phase change material experimentally measured at a duty factor of 0.1 for a) τ_{on} = 2.5 s, b) τ_{on} = 40 s, c) τ_{on} = 400 s. d) Representative thermal impedance of a resistor-capacitor (blue dashed line), illustrating the three characteristic regimes of behavior, as well as the effect of material properties which dominate the thermal impedance within each of those regimes. Data points marked (a), (b), (c) in Fig. 4d represent experimentally measured traces in Fig. 4a, 4b, 4c, respectively.

The existence of melting induces a measurable decrease in thermal impedance relative to the effects of sensible heating (Fig. 5). Thermal impedance is measured in both the case of the reference (empty copper foam), $Z_{\mathrm{th}}^{\mathrm{ref}}$, and for the PCM-infiltrated foam, $Z_{\mathrm{th}}^{\mathrm{pcm}}$. The difference, $Z_{\mathrm{th}}^{\mathrm{ref}} - Z_{\mathrm{th}}^{\mathrm{pcm}}$ (Fig. 5b,d), which will be referred to as the 'thermal impedance suppression', corresponds specifically to the contribution of the latent heat in suppressing the thermal impedance. To isolate the independent contributions of latent heat and sensible heat, the experiment is repeated for $T_0 > T_{\mathrm{m}}$ (Fig. 5a,b), where the PCM remains in the liquid phase, and for $T_0 < T_{\mathrm{m}}$ (Fig. 5c,d) where the PCM begins in the solid

phase and may melt/freeze during heating/cooling cycles. In the case where the PCM remains entirely liquid throughout the experiment, introduction of additional thermal mass moderately decreases the thermal impedance across nearly the entire range of τ_{on} characterized, due to the increased thermal mass. In practice, the additional thermal mass delays the rise to the steady state condition and damps out high frequency responses to the applied heat pulse. For most τ_{on}, the temperature rise at the heated surface is lower. A peak is observed in the relative thermal impedance difference between $\tau_{on} = 10^1$ to 10^2 s that corresponds to the timescale of heat diffusion into the single phase PCM-filled pores (Fig. 5a,b). In the case where melting occurs, introduction of additional thermal mass which melts decreases $Z_{\mathrm{th}}^{\mathrm{pcm}}$ over the range of $\tau_{on} = 10^1$ to 10^3 s, corresponding with the melting within hexadecane-filled pores (Fig. 5c,d). The exact range of conditions under which melting most strongly impacts $Z_{\mathrm{th}}^{\mathrm{pcm}}$ depends on the entire range of conditions, including the thermal boundary conditions, the geometry of the specimen, and the thermophysical properties of the PCM composite.

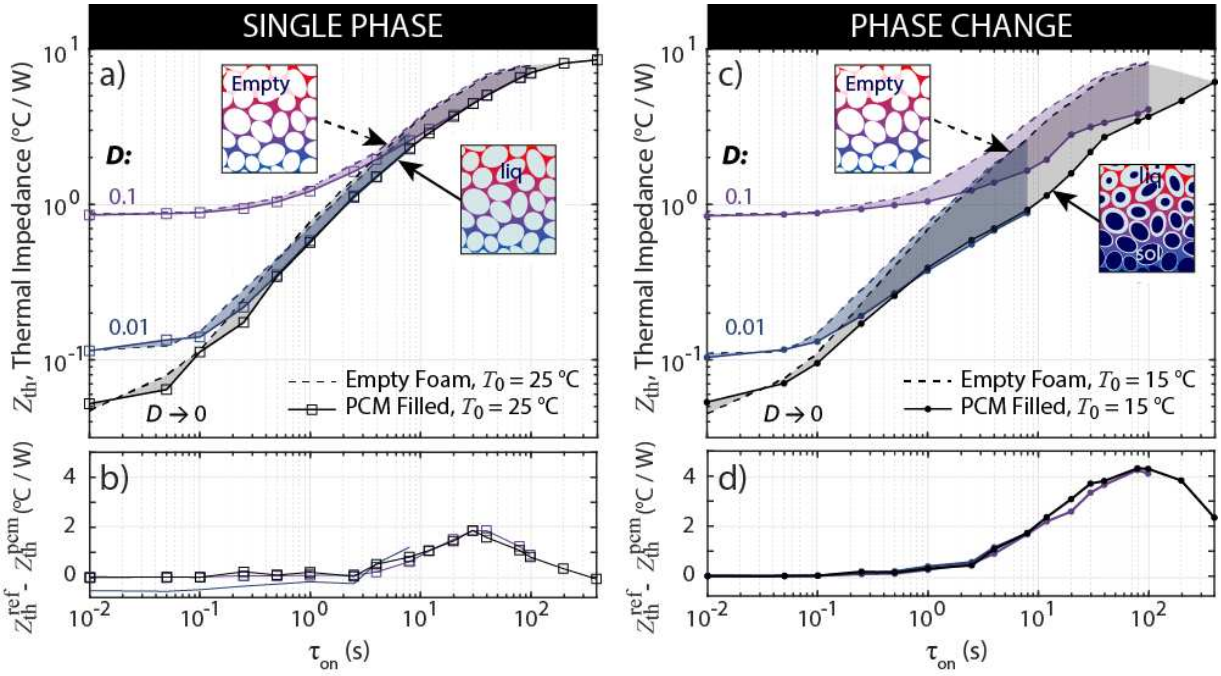

Fig. 5. Thermal impedance of reference empty copper foam, $Z_{\mathrm{th}}^{\mathrm{ref}}$ (dashed lines), and PCM-filled copper foam, $Z_{\mathrm{th}}^{\mathrm{pcm}}$ (solid lines), for a cold temperature of a) T_0 = 25 °C, and c) T_0 = 15 °C, as well as the thermal impedance suppression, $Z_{\mathrm{th}}^{\mathrm{ref}} - Z_{\mathrm{th}}^{\mathrm{pcm}}$ (b,d), which illustrates the impact of introducing PCM into the volume. Measurements are illustrated at duty factors of D = 0, 0.01, 0.1, over a range of τ_{on} = 10^{-2} to $4{\cdot}10^2$. In a), b), $T_0 > T_m$ and therefore melting does not occur. Thus, a), b) illustrate the effect of storing heat via sensible heating of the PCM, whereas c), d) illustrate the effect of storing heat via both sensible heating of the PCM and some contribution from the latent heat of melting. A direct comparison of PCM filled foams at 15 °C and 25 °C is included in Fig. SI-7.

Assessing melting within the composite PCM

As complex heterogeneous media, phase change material composites present unique thermal challenges due to the different time scales associated with heat transfer through the composite slab and with melting of internal PCM-filled pores. If the rate of heat transfer into the composite is sufficiently high, this can result in thermal heterogeneities and incomplete melting (violation of a quasi-1D condition). Thus, measurement of thermal impedance can be deployed as an indirect measure of internal melting behavior by comparing the expected response for a quasi-1D uniform composite material to the experimentally measured thermal impedance of the composite (Fig. 6).

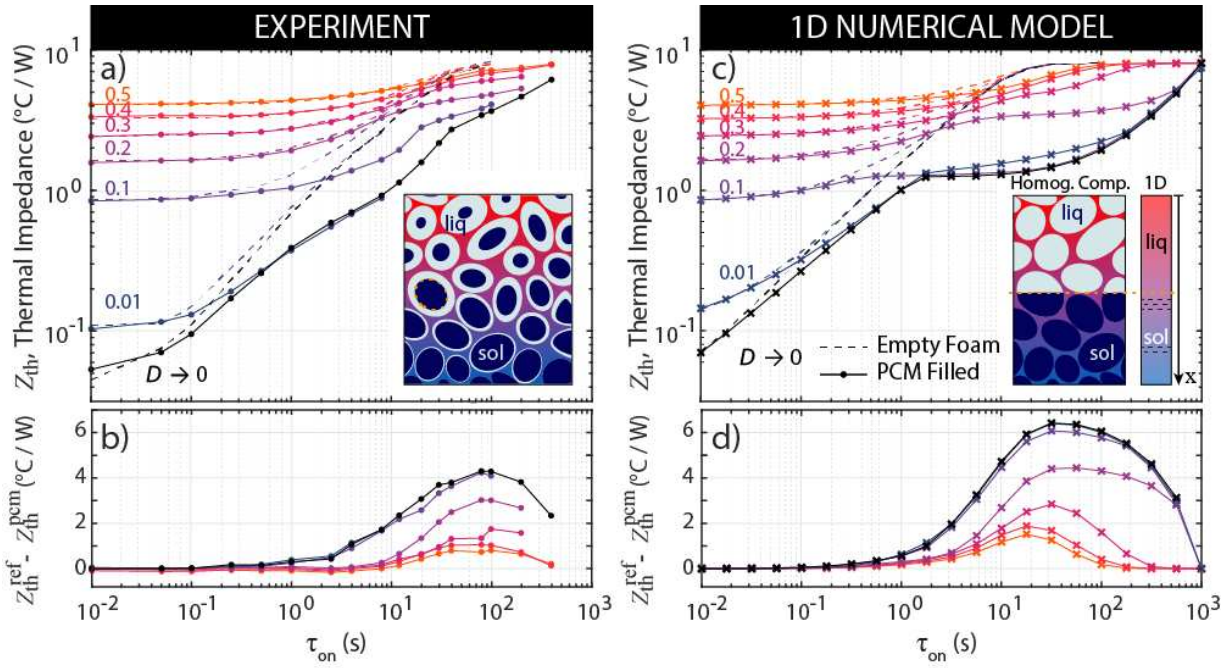

Fig. 6. a), b) Experimental measure and c), d) 1D simulation of (a, c) thermal impedance of empty copper foam, $Z_{\mathrm{th}}^{\mathrm{ref}}$ (dashed lines), and PCM-filled copper foam, $Z_{\mathrm{th}}^{\mathrm{pcm}}$ (solid lines), and (b, d) the thermal impedance suppression $Z_{\mathrm{th}}^{\mathrm{ref}} - Z_{\mathrm{th}}^{\mathrm{pcm}}$. (c, inset) Under the homogeneous composite approximation, a flat melt front propagates vertically through the composite upon heating and cooling, based on the balance of energy at the solid-liquid interface, resulting in a well-defined plateau in the thermal impedance plot (c). (a, inset) Under more realistic assumptions, temperature gradients will exist laterally, within each pore, as a melt or solidification front propagates inwards from the thermally conductive copper lattice, resulting in extended melting over a broader range of time period, and a decrease in the thermal impedance suppression (b).

Comparison of experimentally measured thermal impedance with numerical predictions reveal differences which suggest incomplete melting of the PCM within foam pores. Overall, there is qualitatively good agreement between the range of time scales at which melting impacts the thermal impedance of the composite PCM (τ_{on} = 10^0 to 10^3 s; Fig. 6). However, the numerically predicted impedance curves indicate an abrupt plateau in the thermal impedance when melting occurs, caused by the existence of a sharp melt interface which slowly moves away from the heated surface (Fig. 6c). In contrast, the experimental impedance curves indicate broad distribution of the impact on the thermal impedance, as well as a decrease in the thermal impedance suppression, $Z_{\mathrm{th}}^{\mathrm{ref}} - Z_{\mathrm{th}}^{\mathrm{pcm}}$ (Fig. 6b). This observation is consistent with internal heterogeneous temperature distribution and incomplete melting

within foam pores. Additionally, subtle differences in the numerical model for the short pulses at D = 0 reflect minor deviations, including the non-ideal nature of the serpentine thin-film heater, as well as the high resistance, but not truly adiabatic boundary layer above the heater surface.

The time scale associated with melting of an individual PCM-filled pore, as approximated by the quasi-steady state analytical solution to melting of a sphere, is on the order of 10^1 s, corresponding with the onset of impact on the thermal impedance suppression $Z_{\mathrm{th}}^{\mathrm{ref}} - Z_{\mathrm{th}}^{\mathrm{pcm}}$. Under a constant temperature boundary condition, the quasi-steady state solution to the 1D spherical Stefan problem defines the melt front position as a function of time:

$$\delta(t)\left(1 + r_0 \ln(\delta(t)/r_0)\right) = r_0 + t k_{\mathrm{l}}(T_0 - T_{\mathrm{m}})/(r_0 \Delta H_{\mathrm{vol}}) \qquad \text{Eq. 9}$$

Here, r_0 is the average pore size, k_{l} is the thermal conductivity of liquid hexadecane, and ΔH_{vol} is the volumetric latent heat of fusion. The closure time, defined by $\delta(t) = 0$, is dependent on the temperature difference between T_0 and T_{m}. Assuming a temperature rise on the boundary of 10 to 20 °C, a single pore is fully melted on the order of 10^1 s. Thus, the time scale of melting of an individual pore of a composite PCM is expected to place a lower limit on the time scale of absorbing heat within these heterogeneous composite materials. However, the exact interactions between internal structure of a composite PCM and their impact on thermal impedance remains a subject for further investigation.

At the limit of long pulses, overall energy balance considerations dictate the time at which this slab is entirely melted. Specifically, given the slab thickness, heating power, and PCM thermophysical properties, and neglecting sensible heating effects, complete melting of the slab requires 420 s. In the experimental case, this time scale is observed to correlate well with the maximum in the measured thermal impedance suppression (Fig. 6), although temperature heterogeneity within the composite PCM extends the period of melting beyond this time.

Thermal impedance as a guide to enhancing charging of thermal energy

One of the principal motivating factors behind developing the concept of thermal impedance in PCM systems remains its utility as a measure of internal dynamics in complex systems. Tracking the internal partitioning of heat into latent heat energy storage is challenging to assess accurately experimentally, whereas measuring $Z_{\mathrm{th}}^{\mathrm{pcm}}$, a property that can be recorded from the surface of a volume, provides insight into the transient thermal response of a material, from which its internal dynamics can be deduced. For a particular geometry and structure, the relative amount of heat that is partitioned into latent and sensible heat changes as τ_{on} increases (Fig. 7a,b). Initially, heat is partitioned primarily into sensible heat until the internal temperature of the PCM is raised to its melting temperature. At long periods, heat loss terms begin to dominate the total energy balance, and the both the relative amount of heat stored as latent heat, as well as the thermal impedance suppression, $Z_{\mathrm{th}}^{\mathrm{ref}} - Z_{\mathrm{th}}^{\mathrm{pcm}}$, begin to decrease (Fig. 7a,b).

The storage fraction (Fig. 7c) correlates strongly with both the relative magnitude and the time scale range of the thermal impedance suppression, $Z_{\mathrm{th}}^{\mathrm{ref}} - Z_{\mathrm{th}}^{\mathrm{pcm}}$ (Fig. 7b). In contrast, the marginal utilization of the PCM is primarily a useful indicator of when the latent heat reservoir is exhausted (i.e., the upper limit of the thermal impedance suppression; Fig. 7d). Longer heat periods τ_{on} tend to melt a greater

fraction of the PCM, but relatively less of the input heat is stored as latent heat. This insight is important from an application perspective, regardless of whether the aim is the storage of thermal energy (e.g., a thermal battery), or the mitigation of a temperature rise on a heated surface (e.g., thermal management of an electronic component). From a thermal energy storage perspective, this observation implies that engineering geometric and material parameters to maximize storage fraction, which explicitly takes heat loss terms into account, will result in the greatest fraction of recoverable heat from the energy reservoir, while simultaneously reducing the maximum input temperature to store that heat, which improves overall efficiency of the system. From a thermal management perspective, reducing the thermal impedance is the ultimate objective of the thermal design of the system. At short periods, when heat cannot be rejected from a system at a sufficient rate, adding a reservoir to transiently store heat can result in reducing the maximum temperature rise of a surface.

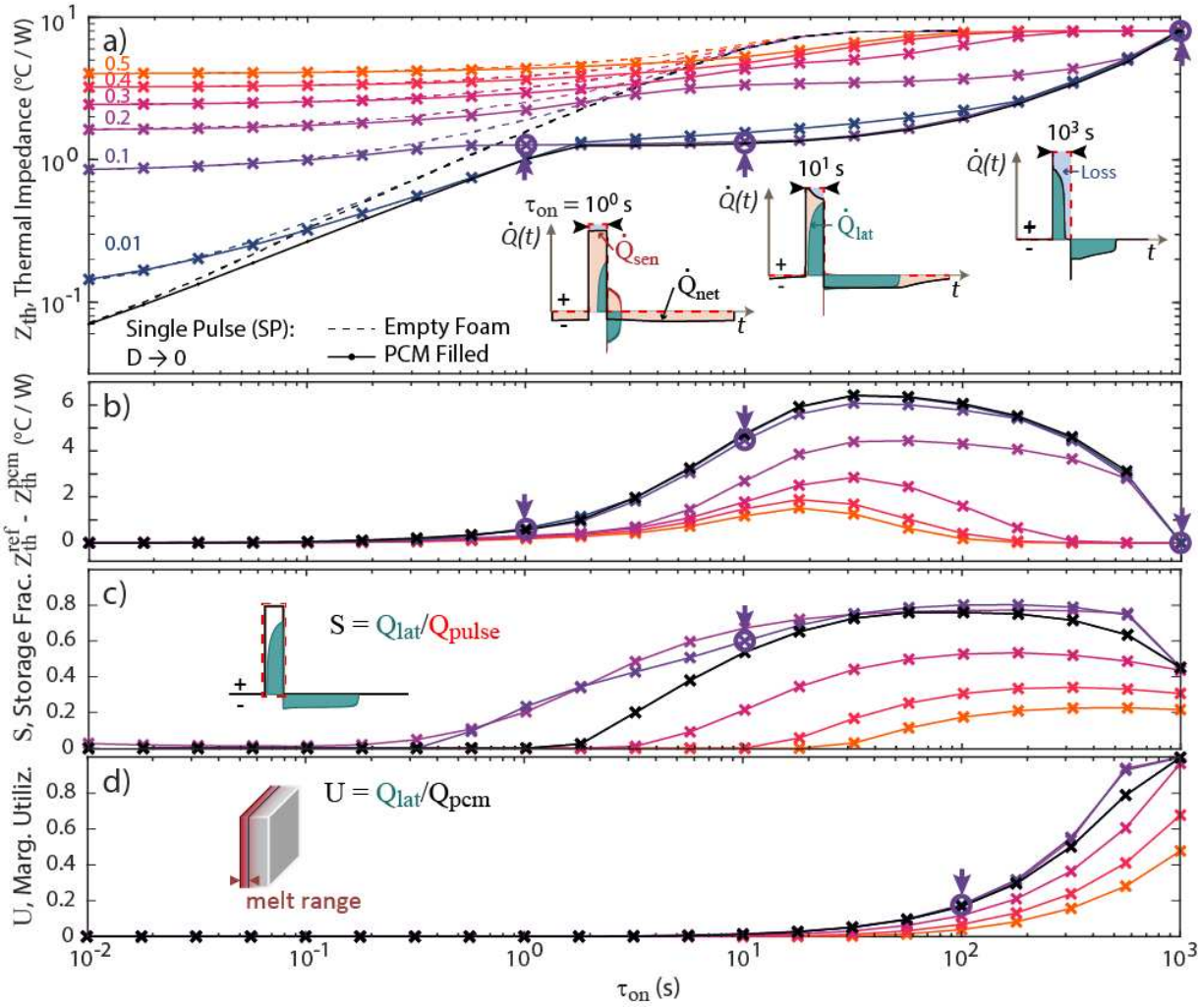

Fig. 7. a) 1D numerical simulation of thermal impedance of empty copper foam, $Z_{\mathrm{th}}^{\mathrm{ref}}$ (dashed lines), and PCM-filled copper foam, $Z_{\mathrm{th}}^{\mathrm{pcm}}$ (solid lines). b) Thermal impedance suppression, $Z_{\mathrm{th}}^{\mathrm{ref}} - Z_{\mathrm{th}}^{\mathrm{pcm}}$. Inset illustrates the change in the relative fraction of heat that is partitioned into sensible and latent heat storage for different τ_{on}. c) Storage fraction, S, and d) Marginal Utilization, U, for the 1D simulation. Purple arrows indicate the conditions illustrated in each inset image. U decreases at higher duty factors because the slab does not have sufficient time to fully recharge (i.e., at the onset of each pulse, a significant volume fraction is already liquid (Fig. SI-8).

Thermal impedance of PCMs in thermal circuits

Thermal energy storage systems generally consist of multiple linear thermal elements (capacitors, resistors) assembled in series and parallel, which can be described in an equivalent thermal circuit. Thus, it is reasonable to assess the ability to combine the characterized thermal impedance of a nonlinear PCM element together with other common linear elements. To evaluate this approach, we consider two simple thermal circuits, consisting of a nonlinear PCM element either in series (on the heater side; Fig. 8a) or in parallel (Fig. 8b) with an ideal massless thermal resistor. These circuits are consider for representative pulsed heater duty factors of D = 0, 0.1.

The series circuit example demonstrates that, under certain limiting conditions, thermal impedance of an overall thermal circuit can be described as a linear combination of elements, even if the circuit contains a nonlinear PCM component (Fig. 8a). In particular, this simple circuit is a useful analog for electronic components, which may exhibit multiple resistive layers of thermally resistive packaging, but which have relatively low thermal capacitance. In contrast, the parallel circuit example demonstrates that the nonlinearity of the PCM dictates the transient thermal response at intermediate time periods (when the melting process plays the largest role). Since the PCM is a nonlinear circuit element, the voltage divider effect of the parallel resistor means that the PCM element is effectively seeing a different boundary condition (lower heat flux into the heated surface), which then changes the impedance characteristic. However, this shortcoming may be overcome by characterizing the PCM component across a range of T_0 and $\dot{Q}_0''$, to account for the impact of other circuit elements on the thermal boundary conditions of the PCM element.

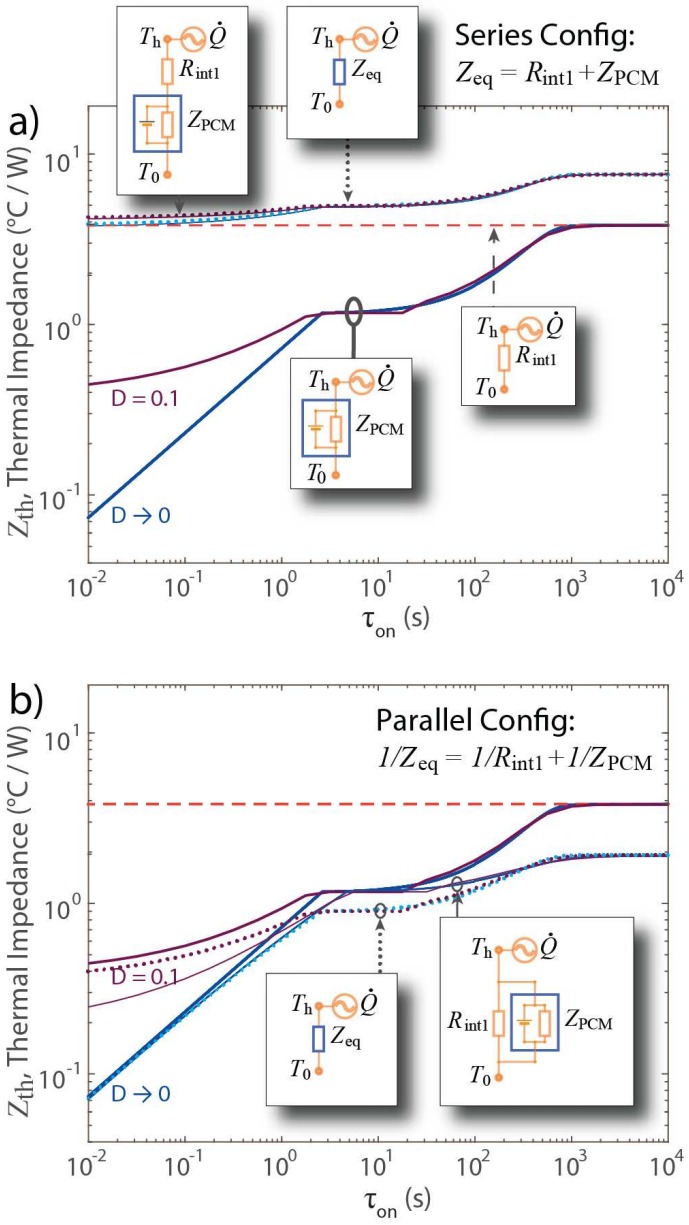

Fig. 8. Numerically calculated thermal impedance for individual elements and for a PCM element a) in series with an ideal massless resistor, and b) in parallel with an ideal massless resistor. Z_{PCM} is shown in bold lines (for the same element as discussed in Fig. 6), massless resistor is shown with dashed red line (which is independent of on time for an ideal massless resistor). The thermal impedance of the complete circuit is evaluated numerically (thin solid line) and is compared against an equivalent impedance which is given as $Z_{eq} = R_{int1} + Z_{PCM}$ for the series configuration, and $Z_{eq}^{-1} = R_{int1}^{-1} + Z_{PCM}^{-1}$. The equivalent impedance converges with the numerically simulated circuit in the series configuration, but diverges over short τ_{on} in the parallel configuration, as discussed in the text. Thermal impedances are calculated for values of D = 0 (blue) and D = 0.1 (purple).

Conclusions

Effective utilization of phase change materials in pulsed periodic systems requires development of a guiding framework to enable design and integration of these highly non-linear components. This framework must build a common language and set of descriptors that can be used to design a thermal energy storage component tailored for a particular end-use application. In this context, thermal impedance is the critical characteristic for determining the transient periodic response to different charge and discharge rates of a thermal storage component. The thermal impedance captures both intrinsic material properties and extrinsic design elements, where the general strategy of a thermal energy storage component is always to minimize thermal impedance under the range of application-oriented operating conditions. For application as an energy storage/retrieval system, minimum impedance enables the most efficient access to the stored heat, with a minimum degree of overheating/undercooling. For application as a thermal buffering system for thermal management, minimum impedance directly represents the most efficient suppression of temperature changes at the heated/cooled surface.

In this manuscript, we have developed the theoretical framework to evaluate the thermal response of PCM layers to periodic unsteady thermal boundary conditions and have experimentally and numerically interrogated the behavior of a model composite PCM system. These experiments have revealed the complex non-linear behavior of composite PCM slabs, but have also identified guidelines that form the basis of design of PCM components for pulsed energy systems. Specifically, to significantly decrease the thermal impedance of the system, a PCM slab must maximize the storage fraction, S (the quantity of heat stored as latent heat, relative to the total pulse of heat), while not exceeding the overall capacity of the slab, as measured by its marginal utilization, U (the extent of melting that occurs during each pulse).

It is our hope that developing this analytical framework will introduce a common vocabulary and toolset for analysis and design of thermal energy storage components intended for pulsed periodic power thermal energy storage. Specifically, this approach already provides an avenue to further evaluate the effects of intrinsic PCM material properties, composite PCM mesoscale structure, and the critical length scales associated with a composite structure on the transient periodic thermal response of a PCM slab. Thus, this approach can form the basis for both optimal design of PCM components under a known periodic thermal load, or, by analogy with high power electronics packages, as a descriptive specification for a standalone component, which can then be impedance matched with other components of the overall thermal system. Only through adopting such a unifying framework can we hope to advance the effective design of thermal energy storage components for pulsed power applications.

Methods

Materials

The metallic thermally conductive matrix used in this study was a 1.07 cm thick copper foam with a 96.7% porosity (ϕ) and 30.6 pores per inch (PPI) (Fig. SI-1, 2). All samples had dimensions of 2.44 cm in

length and width. The PCM material chosen was 99% pure hexadecane (Sigma-Aldrich) with a melting point (T_{melt}) of 17.4 °C and a gravimetric latent heat of fusion (ΔH_w) of 226.5 J·g^{-1} measured using a TA Q2000 Differential Scanning Calorimeter at a heating rate of 2 °C·min^{-1} (Fig. SI-9).

Experimental Setup and Sample Preparation

The dynamic system consists of a quasi-one-dimensional system with a heat flux boundary applied by a thick film heater on an insulated (quasi-adiabatic) top surface (Fig. 3). The heat flux boundary condition is regulated by a 32 W Programmable DC power supply (Keysight B2961A) connected to a thick film polyimide-coated heater (Omega Heater KHLVA-101/10). On the bottom surface is a quasi-isothermal cooling boundary condition controlled by a mini-channel cold plate (Advanced Thermal Solutions ATS-CP-1002; 0.005 °C·W^{-1} at 4 L·min^{-1}). This cold plate is connected to a (14.8 L·min^{-1}) water chiller (PolyScience LS51M11A110C) with a T_0 of 10, 15, or 25 +/-0.1 °C. The data acquisition (DAQ) system consisted of a National Instruments DAQ-9174 combined with a TB-9212 Isothermal Terminal Block and a 9252 Voltage Input Block. Three fine-wire (0.08 mm diameter) K-type thermocouples (Omega 5SC-TT-K-40-36-ROHS) are used to collect temperature data. One thermocouple is fixed to the foil using conductive epoxy at the center beneath the heater (T_h), one is fixed to the cold plate (T_0) adjacent to the sample to avoid adding additional thermal resistance to the cold plate/sample interface. Polyimide tape is used to fix the thermocouple on the cold plate, and fiberglass insulation is placed on top for insulation. A final thermocouple measures the ambient temperature of the lab (T_{amb}). The thermocouples are calibrated to within 0.1 °C to ensure data accuracy.

Each sample was prepared with layers to enhance one-dimensional heat transfer and reduce interfacial resistances (R_{int}). Because of the copper foam's topology, the thermal conduction path at the surface with the heater and the cold plate is inhibited by a low contact surface area due to the foam's ligaments. Therefore, a layer of aluminum foil was used as a heat spreader and was fixed by silver conductive epoxy (EPO-TEK® H20E; 2.5 W·m^{-1}·°C^{-1} from laser flash analysis (LFA) and 29 W·m^{-1}·°C^{-1} from thermal resistance data)[43] at the interface between the heater and the sample and the cold plate and the sample. Approximately 0.6 g of silver epoxy (Arctic Silver 5 AS5-3.5G; 0.94 to 1 W·m^{-1}·°C^{-1})[44,45] was applied at each interface to ensure the metal foam struts had sufficient thermal contact with the foil. To mount the sample onto the insulating holder, 0.3 g of thermal paste was applied to the sample's bottom interface using a quincunx pattern. In addition, to prevent PCM and silver thermal paste contamination, the heater was attached to the sample/foil by adding a layer of silver conductive epoxy. The high-temperature hot-melt adhesive was applied around the sample's bottom edges to shield the paste from mixing with the PCM. An acrylonitrile butadiene styrene (ABS) sample holder fabricated using a Stratasys F370 printer is fixed to the cold plate with silicone adhesive to contain liquid PCM and to reduce heat loss to the environment. The total thermal resistance (R_{total}) was 8.45 ± 0.07 °C·W^{-1} for the empty foam, and 8.89 ± 0.14 °C·W^{-1} for the filled foam. This variation is within measurement uncertainty and likely represents subtle differences in contact between the irregular foam boundary and the flat heater and cold plate surfaces. The reported R_{foam} from literature was 3.74 °C·W^{-1}, and the combined R_{int} was 5.15 °C·W^{-1} (empty) and 5.19 °C·W^{-1} (filled).

An insulating silicone open-cell foam wrapped in polyimide tape was placed on top of the sample to reduce heat loss from the top surface. To minimize thermal contact resistances associated with the various interfaces, a 2.2 N weight is placed on top to provide a consistent compressive force across all experiments.

Data Collection and Processing

A LabVIEW program controlled the power supply and recorded temperature and voltage readings from the setup. Two testing modes were used: stepwise and pulse train power inputs. Temperatures and voltages were recorded at a sampling rate of 300 Hz. This results in 6 data points collected per period at duty factors of 0.5 at on-time of 0.01 s, or for 300 data points at the same on-time but at a duty factor of 0.01. The duration of each run varied depending on the testing mode to allow the system to reach a steady state. For the stepwise runs, the power varied from 0 to 5.8 W. For the pulse trains, a constant power of 2.6 W (i.e., 0.43 W·cm^{-2}) was applied using a 0 V lower level and a 14 V peak level input with a 76.0 Ω resistance from the polyimide heater. For each run, the heater applies a pulsed thermal input, where the pulse train's duty factor (D) and on times (τ_{on}) are an array input to the program.

Temperature profiles (T_h, T_0, and T_{amb}) were collected for each sample and analyzed using MATLAB. For the stepwise case, the temperature rise is measured using the difference between the steady-state, hot-side temperature at each power level and cold-side temperature. For the pulse train case, the periodic unsteady thermal response is allowed to reach sufficient cycles to reach a convergent periodic thermal response at each combination of duty factor and on-time. A script was used to identify the maximum temperature rise for the last 30% of the collected convergent periodic responses. The reported hot-side temperature (T_h) is the mean value of the last 30% peaks. The ambient temperature, T_{amb}, was measured during each experiment, but was not observed to cause significant deviations between runs.

Numerical Simulation

In this work, numerical investigations are utilized to characterize heat transfer and, specifically, the thermal impedance, Z_{th}, marginal utilization, U, and storage fraction, S, of the composite PCM slab under pulsed periodic heat flux boundary conditions (Fig. 6, 7). We use 1D finite difference analysis (FDA) models simulating conductive heat transfer through Cartesian PCM composite geometries, which have been established and validated in previous publications.[34,40,41] The fundamental assumptions of the FDA models are: 1) the material properties of the solid and liquid phases are temperature independent, 2) melting occurs at a singular temperature, 3) the interface between phases is well defined, 3) the densities of the solid and liquid phases are equal leading to no mass transfer upon phase change and 4) no convection occurs in the liquid phase. Within the FDA, nodes are linearly spaced between boundaries and node characteristics are given by the system geometry and effective properties, treating the system as a composite material slab. For all simulations executed in this work, the pulsed periodic boundary condition is cycled sufficiently to achieve periodic unsteady conditions; boundary conditions are applied for at least 10 cycles, and until the periodic transient thermal response converges (defined as $(T_{\max}^{\mathrm{n+1}} - T_{\max}^{\mathrm{n}})/T_{\max}^{\mathrm{n+1}} < 10^{-4}$). For every timestep, the heat transfer between nodes is calculated using an implicit backward Euler method, from which the temperature and melt fraction of each node is determined. To this end, for a Cartesian coordinate basis the heat equation is given by:

$$\frac{1}{\partial x}\left(k\frac{\partial T}{\partial x}\right) = \rho C_{\mathrm{p}}\frac{\partial T}{\partial t} + \Delta H_{\mathrm{vol}}\frac{\partial f}{\partial t} \qquad \text{Eq. 8}$$

where x, ρ, C_{p}, T, t, k and ΔH_{vol} represent distance, density, specific heat capacity, temperature, time, thermal conductivity, and volumetric latent heat, respectively. The melt fraction of a given node volume

is represented by f, where possible values range from 0, which represents not at all melted, to 1, which represents completely melted, with intermediate values represent partial melting. Within Eq. 8, the left-hand side of the equation represents the rate of heat transfer through the given volume and the right-hand side of the equation represents the heat absorbed by the volume through sensible (term 1) and latent (term 2) heating. Within the FDA, once the melting temperature of a given node is reached, the node will absorb thermal energy into the latent heat until the volume is completely melted before beginning to sensibly heat leading to a singular well-defined front.

Resolution of the FDA model is dependent on timestep length and node spacing. Time steps are chosen to be 10^4 time steps per total period, which provides sufficient temporal resolution, even at low duty factors. A total of 1001 nodes are distributed between the two boundaries of the simulated volume (total height of 10.7 mm), resulting in spacings of 10.7 μm between nodes. This combination of values yields results in thermal impedance which converge within <1 %. Accuracy of the resulting finite difference model was validated against ANSYS simulations, analytical models, and experimental data; these results are reported elsewhere.[40,41] Additionally, the numerical model converged to analytical solutions for the from the single pulse limit (D = 0; Fig. SI-10, SI-11).

Data availability

The authors declare that the data supporting the findings of this study are available within the paper and its Supplementary Information files. Should any raw data files be needed in another format, they are available from the corresponding author upon reasonable request.

References

1 Li, Q. *et al.* High-temperature dielectric materials for electrical energy storage. *Annual Review of Materials Research* **48**, 219-243 (2018).

2 Tian, R. *et al.* Quantifying the factors limiting rate performance in battery electrodes. *Nature communications* **10**, 1933 (2019).

3 DeTeresa, S. Materials for advanced flywheel energy-storage devices. *MRS bulletin* **24**, 51-56 (1999).

4 Kiyabu, S., Girard, P. & Siegel, D. J. Discovery of Salt Hydrates for Thermal Energy Storage. *Journal of the American Chemical Society* **144**, 21617-21627 (2022).

5 Ammann, J., Michel, B., Studart, A. R. & Ruch, P. W. Sorption rate enhancement in SAPO-34 zeolite by directed mass transfer channels. *International Journal of Heat and Mass Transfer* **130**, 25-32 (2019).

6 Narayanan, S. *et al.* Thermal battery for portable climate control. *Applied energy* **149**, 104-116 (2015).

7 Zhang, X. *et al.* Multiscale understanding and architecture design of high energy/power lithium-ion battery electrodes. *Advanced Energy Materials* **11**, 2000808 (2021).

8 Kang, B. & Ceder, G. Battery materials for ultrafast charging and discharging. *Nature* **458**, 190-193 (2009).

9 Amin, K., Ashraf, N., Mao, L., Faul, C. F. & Wei, Z. Conjugated microporous polymers for energy storage: Recent progress and challenges. *Nano Energy* **85**, 105958 (2021).

10 Shamberger, P. J. & Fisher, T. S. Cooling power and characteristic times of composite heatsinks and insulants. *International Journal of Heat and Mass Transfer* **117**, 1205-1215 (2018).

11 Yazawa, K., Shamberger, P. J. & Fisher, T. S. Ragone relations for thermal energy storage technologies. *Frontiers in Mechanical Engineering* **5**, 29 (2019).

12 Woods, J. *et al.* Rate capability and Ragone plots for phase change thermal energy storage. *Nature Energy* **6**, 295-302 (2021).

13 Qu, D. *et al.* Electrochemical impedance and its applications in energy-storage systems. *Small Methods* **2**, 1700342 (2018).

14 Chang, B.-Y. & Park, S.-M. Electrochemical impedance spectroscopy. *Annual Review of Analytical Chemistry* **3**, 207-229 (2010).

15 Wang, S. *et al.* Electrochemical impedance spectroscopy. *Nature Reviews Methods Primers* **1**, 41 (2021).

16 Qu, D., Ji, W. & Qu, H. Probing process kinetics in batteries with electrochemical impedance spectroscopy. *Communications Materials* **3**, 61 (2022).

17 Kawka, P., De Mey, G. & Vermeersch, B. Thermal characterization of electronic packages using the Nyquist plot of the thermal impedance. *IEEE Transactions on Components and Packaging Technologies* **30**, 660-665 (2007).

18 Vintrou, S., Laraqi, N. & Baïri, A. Calculation and analysis of thermal impedance of microelectronic structures from analytical models. *Solid-State Electronics* **67**, 45-52 (2012).

19 Singh, S. *et al.* Effects of die-attach voids on the thermal impedance of power electronic packages. *IEEE Transactions on Components, Packaging and Manufacturing Technology* **7**, 1608-1616 (2017).

20 Fleckenstein, M., Fischer, S., Bohlen, O. & Bäker, B. Thermal Impedance Spectroscopy-A method for the thermal characterization of high power battery cells. *Journal of Power Sources* **223**, 259-267 (2013).

21 Barsoukov, E., Jang, J. H. & Lee, H. Thermal impedance spectroscopy for Li-ion batteries using heat-pulse response analysis. *Journal of power sources* **109**, 313-320 (2002).

22 Li, Z. & Mei, B.-A. Complex thermal analysis of supercapacitor by thermal impedance spectroscopy. *Thermochimica Acta* **710**, 179175 (2022).

23 Papagiannopoulos, I. *et al.* Behaviour of the thermal impedance of buried power cables. *International Journal of Electrical Power & Energy Systems* **44**, 383-387 (2013).

24 Xu, J., Wang, R. & Li, Y. A review of available technologies for seasonal thermal energy storage. *Solar energy* **103**, 610-638 (2014).

25 Schmidt, T., Mangold, D. & Müller-Steinhagen, H. in *ISES solar world congress.* 2003.

26 Vadiee, A. & Martin, V. Thermal energy storage strategies for effective closed greenhouse design. *Applied energy* **109**, 337-343 (2013).

27 Reuss, M., Beck, M. & Müller, J. Design of a seasonal thermal energy storage in the ground. *Solar energy* **59**, 247-257 (1997).

28 Palacios, A., Barreneche, C., Navarro, M. & Ding, Y. Thermal energy storage technologies for concentrated solar power–A review from a materials perspective. *Renewable Energy* **156**, 1244-1265 (2020).

29 Pelay, U., Luo, L., Fan, Y., Stitou, D. & Rood, M. Thermal energy storage systems for concentrated solar power plants. *Renewable and Sustainable Energy Reviews* **79**, 82-100 (2017).

30 Yu, Z. J., Huang, G., Haghighat, F., Li, H. & Zhang, G. Control strategies for integration of thermal energy storage into buildings: State-of-the-art review. *Energy and Buildings* **106**, 203-215 (2015).

31 Kamal, R., Moloney, F., Wickramaratne, C., Narasimhan, A. & Goswami, D. Strategic control and cost optimization of thermal energy storage in buildings using EnergyPlus. *Applied Energy* **246**, 77-90 (2019).

32 De Bock, H. P. *et al.* A system to package perspective on transient thermal management of electronics. *Journal of Electronic Packaging* **142**, 041111 (2020).

33 Gurrum, S. P., Joshi, Y. K. & Kim, J. Thermal management of high temperature pulsed electronics using metallic phase change materials. *Numerical Heat Transfer, Part A: Applications* **42**, 777-790 (2002).

34 Tamraparni, A. *et al.* Design and optimization of lamellar phase change composites for thermal energy storage. *Advanced Engineering Materials* **23**, 2001052 (2021).

35 Hoe, A. *et al.* Objective oriented phase change material composite heat sink design. *Applied Thermal Engineering* **209**, 118235 (2022).

36 Tamraparni, A. *et al.* Design and optimization of composite phase change material for cylindrical thermal energy storage. *International Journal of Heat and Mass Transfer* **208**, 123995 (2023).

37 Bedoya, A. *et al.* Thermal impedance. *European Journal of Physics* **42**, 065101 (2021).

38 Shamberger, P., Hoe, A., Deckard, M. & Barako, M. Dynamics of melting in a slab under harmonic heating and convective cooling boundary conditions. *Journal of Applied Physics* **128** (2020).

39 Casano, G. & Piva, S. Experimental and numerical investigation of the steady periodic solid–liquid phase-change heat transfer. *International Journal of Heat and Mass Transfer* **45**, 4181-4190 (2002).

40 Deckard, M. E., Felts, J. & Shamberger, P. J. in *2018 17th IEEE Intersociety Conference on Thermal and Thermomechanical Phenomena in Electronic Systems (ITherm).* 109-116 (IEEE).

41 Hoe, A. *et al.* Conductive heat transfer in lamellar phase change material composites. *Applied Thermal Engineering* **178**, 115553 (2020).

42 Lide, D. R. *CRC handbook of chemistry and physics*. Vol. 85 (CRC press, 2004).

43 Technology, E. *Epo-Tek H20E Technical Data Sheet*, <https://www.epotek.com/docs/en/Datasheet/H20E.pdf> (2024).

44 Narumanchi, S., Mihalic, M., Kelly, K. & Eesley, G. in *2008 11th Intersociety Conference on Thermal and Thermomechanical Phenomena in Electronic Systems.* 395-404 (IEEE).

45 Warzoha, R. J. & Donovan, B. F. High resolution steady-state measurements of thermal contact resistance across thermal interface material junctions. *Review of Scientific Instruments* **88**, 094901 (2017).

Acknowledgements

This material is based upon research supported by, or in part by, the U. S. Office of Naval Research under award number N00014-17-1-2802.

Author information

Authors and Affiliations

Department of Materials Science and Engineering, Texas A&M University, College Station, TX, 77843, USA

Juan C. Lago, Veronica Gonzalez, Alison Hoe, Patrick J. Shamberger

NG Next Basic Research Laboratory, Northrop Grumman Corporation, Redondo Beach, CA, 90278, USA

Michael Barako

Contributions

J.C.L. and V.G. fabricated the experimental setup, collected and interpreted experimental data, and contributed to the initial draft of the manuscript. A.H. conceived the experimental setup and characterized the copper foam. M.B. developed analytical framework, including the series solution, and contributed to the conceptual design of the experiment and revised the manuscript. P.J.S. contributed the finite difference results, supervised the project, and revised the manuscript.

Corresponding Author

Correspondence to Patrick J. Shamberger.

Ethics declarations

Competing Interests

The authors declare no competing interests.

Supplementary information

Supplementary Information

Supplementary Figs. 1–7, Table 1, and References. These figures include detailed characterization of the copper foam, examples of experimentally measured temperatures and thermal impedance data, calorimetry data of the PCM, and parameters used in 1D finite difference thermal modeling.